Acta of Bioengineering and Biomechanics
Vol. 14, No. 4, 2012

Review article
DOI: 10.5277/abb120414

Spectroscopic techniques in the study of human tissues and their components. Part II: Raman spectroscopy

SYLWIA OLSZTYŃSKA-JANUS[1,2]*, MARLENA GĄSIOR-GŁOGOWSKA[1,2], KATARZYNA SZYMBORSKA-MAŁEK[3], MAŁGORZATA KOMOROWSKA[1,2], WOJCIECH WITKIEWICZ[2], CELINA PEZOWICZ[2,4], SYLWIA SZOTEK[4], MAGDALENA KOBIELARZ[2,4]

[1] Institute of Biomedical Engineering and Instrumentation, Wrocław University of Technology.
[2] Regional Specialist Hospital in Wrocław, Research and Development Centre, Wrocław.
[3] Institute of Physical and Theoretical Chemistry, Wrocław University of Technology.
[4] Division of Biomedical Engineering and Experimental Mechanics, Wrocław University of Technology, Poland.

Among the currently used methods of monitoring human tissues and their components many types of research are distinguished. These include spectroscopic techniques. The advantage of these techniques is the small amount of sample required the rapid process of recording the spectra, and most importantly in the case of biological samples – preparation of tissues is not required. In this work vibrational spectroscopy: ATR-FTIR and Raman spectroscopy will be used. Studies are carried out on tissues: tendons, blood vessels, skin, red blood cells and biological components: amino acids, proteins, DNA, plasma, and deposits.

Key words: *vibrational spectroscopy, ATR–FTIR, Raman, tissues*

1. Introduction

ATR-FTIR (Attenuated Total Reflection Fourier Transform Infrared) and Raman spectroscopy are novel tools of modern biology and medicine. Vibrational spectroscopic methods are widely used in studies ranging from single cells to whole tissues analysis. The greatest benefits of these spectroscopic techniques lie in their high sensitivity to biochemical changes, as well as in non-destructive application.

The methods and the application of infrared spectroscopy are described in previous part [1]. A major goal of this paper is the discussion on possibility of an application of Raman spectroscopy in human tissue and their components studies.

2. Raman spectroscopy

Raman spectroscopy is a modern measurement technique used for investigating biological materials, including human tissues. It provides information about their structure at a molecular level and is utilized in medicine as a diagnostic technique. With the use of Raman spectroscopy, tissue changes due to disease processes and pathological factors can be analyzed. The technique is considered as non-invasive and can be used for *in vivo* measurements [2]–[11].

The consequences of disease and aging processes are changes in the biochemical structure of tissues, which are also seen in their Raman spectra [5], [12]. One of more commonly investigated tissues is skin.

* Corresponding author: Sylwia Olsztyńska-Janus, Institute of Biomedical Engineering and Instrumentation, Faculty of Fundamental Problems of Technology, Wrocław University of Technology, Plac Grunwaldzki 13, 50-377 Wrocław, Poland. Tel.: +48 71 320 44 61, fax.: +48 71 327 77 27, e-mail: sylwia.olsztynska-janus@pwr.wroc.pl

Received: March 8th, 2012
Accepted for publication: July 16th, 2012

2.1. Tissues

2.1.1. Skin

The skin is an organ that can be treated as a multilayered material. The histological structure of the skin is not uniform and depends not only on genetic factors, but also the region of the body. The most significant differences are visible in skin thickness in both the epidermis and dermis layers. The epidermis is approx. 0.1 mm thick, whereas the dermis is approx. 1–4 mm thick [13], [14].

The mechanical properties of the skin are mostly determined by the dermis layer. The dermis is composed of two layers, the papillary and reticular dermis. The dermis is a complex system of insoluble fibres (collagen and elastin) and soluble macromolecules (proteoglycans and hyaluronan). The fibrous components resist tensile forces, whereas the soluble macromolecules resist or dissipate compressive forces [15].

Proteoglycans are the biological matrix of collagen fibres and proteoglycan content stimulates collagen fibre synthesis.

In young people collagen fibres in the papillary dermis take the form of densely packed, thin, and irregularly arranged plexuses while in the reticular dermis they take the form of larger, loosely arranged, intertwined, and wavy bundles. With age the amount of collagen fibres increases, which also reduces space between individual fibres. Collagen fibres composed of collagen types I and III are present in both the papillary dermis and the reticular dermis, with the ratio of type III to type I being slightly higher in the papillary layer than in the reticular layer, where type I collagen constitutes approx. 80–90% of the total collagen content. With age collagen fibres show a denser and less twisted arrangement [16], [17].

Elastic fibres are important structural elements. They are made up of two components: the amorphous fraction representing 90% of the mature fibre and composed exclusively of elastin and the microfibrillar component consisting of 10- to 12-nm diameter fibrils [18]. The elastic tissue in the normal skin consists of superficial microfibril bundles, which gradually thicken and merge with increasingly large amounts of amorphous elastin as the papillary dermis changes into the reticular dermis. The relative volume of elastin fibres increases from 0.7% to 2.5% and their diameter grows from 1–2 μm. With age the concentration of elastin fibres in the papillary dermis decreases. Elastic fibres from the skin of older individuals lose some of their elasticity, thicken into clumps, and fray [17].

The mechanical properties of the skin depend on the arrangement and orientation of collagen fibres and surface stresses forming on its surface relative to the distribution of the Langer's lines. These lines are the areas of decreased stress and are arranged perpendicularly to the long axes of the muscles [19]–[22].

Raman spectroscopy provides information about skin structure at a molecular level. Raman spectra of human skin are characterized by the presence of fluorescence background with the height increasing with melanin content in skin [24], [25]. The Raman spectrum of skin is dominated by vibrational bands of its structural proteins and lipids (figure 1a, table 1).

In the range of 3200–3600 cm^{-1}, the Raman spectrum of skin shows a broad band associated with the ν(OH) vibrations of tissue water and the ν(NH) vibrations of proteins [23], [26], [27]. An intense, asymmetric band with the maximum at 2938 cm^{-1} is the band corresponding to stretching vibrations of the CH_2 and CH_3 amino acid side chains as well as the lipid chains, whereas an intense band with the maximum at around 1450 cm^{-1} corresponds to their deformation vibrations [23], [25]–[29]. In the 1200–1700 cm^{-1} range, the amide bands associated with vibrations of amide bonds in polypeptide chains are observed. The amide I band is dominated by the ν(C=O) vibrations, while the amide III band – by the ν(C–N) and δ(N–H) vibrations. In the Raman spectrum of human epidermis, the maximum of amide I band is located at around 1652 cm^{-1}, which is typical of mammalian keratins with the mainly alpha-helical conformation [26], [28], [30]. In the Raman spectrum of entire skin, the maximum of this band is seen at higher wavenumbers of ~1658 cm^{-1}. The 1658 cm^{-1} band primarily corresponds to collagen type I [2], [31], [32]. Within the amide III band, there are two maxima seen in the skin spectrum: 1271 cm^{-1} (assigned to nonpolar fragments with high proline content that form a typical collagen triple helix) and 1244 cm^{-1} (assigned to polar fragments of collagen characterized by low proline content) [2], [5], [27], [34], [35]. Vibrations observed within the 1050–1150 cm^{-1} region are mainly assigned to the ν(C–C) modes from lipid components of the tissue [23], [24], [26], [29]. The bands at 935 and 817 cm^{-1} arise from the skeletal C–C stretching vibrations of proteins [23], [29], [35], [36], [38]. Spectral features in the 450–1050 cm^{-1} region are attributed to aminoacids: 1003 cm^{-1} (phenylalanine), 919 cm^{-1} (proline), 877 cm^{-1} (hydroxyproline, tryptophan), 855 cm^{-1} (proline, tyrosine) [5], [26], [31], [34], [36], [39]. The stretching vibrations of the S–S bonds of cystine are visible in the 510–545 cm^{-1} region [23], [26], [28], [35]. The

1108 and 526 cm^{-1} bands arise from desmosine and isodesmosine amino acids [5].

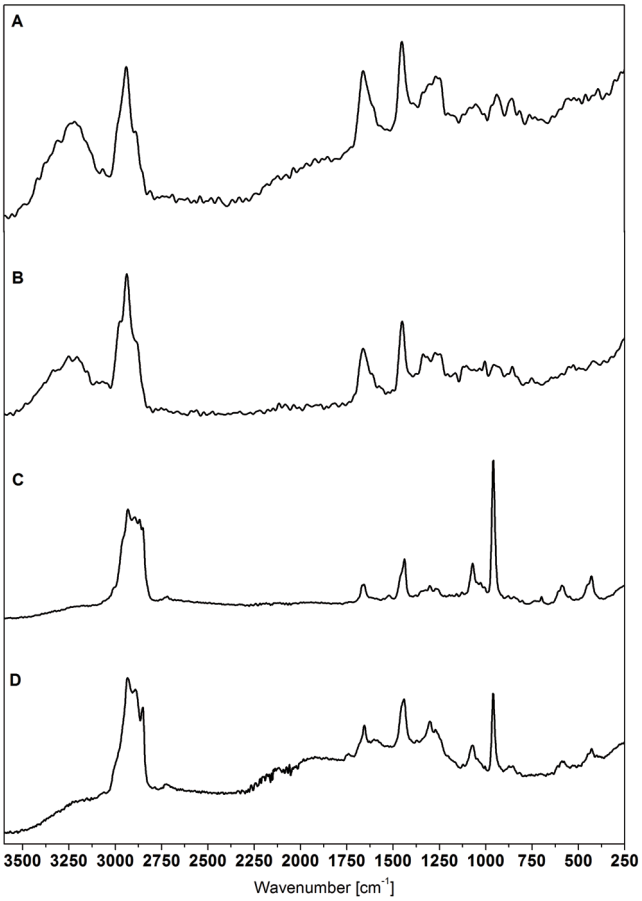

Fig. 1. Representative Raman spectra of human tissues: (a) arm skin; (b) an intact artery; (c) calcified plaque; (d) bone (femur). (FT Raman Bruker RFS/100, Nd:YAG: 1064 nm, 450 mW, 128 scans, 4 cm^{-1})

Table 1. Major positions (in cm^{-1}) and tentative assignment of Raman bands of human arm skin [40]

ν [cm^{-1}]	Assignments*	
3600–3200	ν(OH), ν(NH)	proteins
2938	$\nu(CH_2, CH_3)$	proteins
1657	δ(NH), ν(CO)	amide I proteins
1450	$\delta(CH_2, CH_3)$	lipids and proteins
1271	δ(NH), ν(CN), ν(C–C)	amide III proteins
1244		
1004	$\Delta(C–C)_{ring}$	Phe
935	ν(C–C)	proteins
919	ν(C–C)	Pro
877	ν(C–C), δ(CCH)	Hypro, Trp
855	ν(C–C), δ(CCH)	Pro, Tyr
817	ν(C–C)	proteins
510–545	ν(S–S)	Cys_2

* Abbreviations: ν, stretching; δ, bending; Δ, breathing mode; Phe, phenylalanine; Pro, proline; Hypro, hydroxyproline; Trp, tryptophan; Tyr, tyrosine; Cys_2, cystine.

Vibrational spectroscopic methods are useful for identification of many skin diseases that are difficult to diagnose based only on their clinical manifestation.

Many publications focus on spectroscopic investigations regarding psoriatic skin. It has been demonstrated that psoriatic epidermis contains less lipids compared to healthy tissue. The Raman spectrum of psoriatic skin shows reduced intensity of the $\nu(CH_2)$ vibrational bands (2883 and 2852 cm^{-1}) and disappearance of the bands at 1082 cm^{-1} and 1062 cm^{-1} connected with the skeletal vibrations ν(CC) of lipid chains, whereas the band corresponding to the $\nu(CH_2)$ vibrations of keratin (2872 cm^{-1}) is more intense [28].

As skin cancer is one of the most common cancer types in the world and its early diagnosis is crucial for effective treatment, reliable diagnostic methods, safe for a patient, are continually being searched and Raman techniques are of great interest [41]–[44]. For instance, the Raman spectrum of melanoma is characterized by increased intensity of the lipid vibrational band at 1310 cm^{-1}, while for basal cell carcinoma, the increased band intensity is observed at around 1330 cm^{-1} [42]. In certain types of cancer, higher levels of skin hydration are also observed. The amount of protein-bound water can be estimated based on the Raman spectrum through calculating the ratio of protein ν(CH) (2940 cm^{-1}) to water ν(OH) (3250 cm^{-1}) vibrational band intensities [45]. The analysis of Raman spectra of skin after sunlight exposure has shown that the total amount of water in tanned skin is higher than in untanned skin by about 30% [23]. It has been observed that water content in skin generally increases with age [46]. The evidence of unbound water (tetrahedral water clusters) presence in skin is the band at 180 cm^{-1} in the Raman spectrum [45]. Each skin layer shows a different hydration level [41], [47].

Skin aging processes lead to conformational changes of its structural proteins. In the Raman spectra of old skin and skin exposed to sunlight, shifts of the amide I and III band maxima towards lower frequencies compared to the spectrum of healthy, untanned skin are observed. Moreover, the amide band intensities are reduced and a shift of the $\nu(CH_2)$ band corresponding to aliphatic side chains of amino acids towards lower frequencies, suggestive of protein folding changes, is observed.

In the Raman spectrum of pilomatrixoma, a clear $\nu(PO_4^{3-})$ vibration band (960 cm^{-1}), not observable in healthy skin, is seen [34], [48]. The presence of this band in the Raman spectrum is the basis for diagnos-

tics of atherosclerotic processes within blood vessel walls.

2.1.2. Blood vessel walls

Blood vessel walls are composed of three structurally different, concentric layers: the inner layer (*tunica intima*), the middle layer (*tunica media*), and the outer layer (*tunica adventitia* or *tunica externa*). Histologically, each of the layers is a heterogeneous material, whose structure also varies depending on the topographic location of the blood vessel in the cardiovascular system as well as the age and condition of the patient [49]. The characteristic structure of blood vessel walls provides them with appropriate strength and elasticity, enabling their smooth functioning with respect to the transfer of loads generated by arterial blood flow [50].

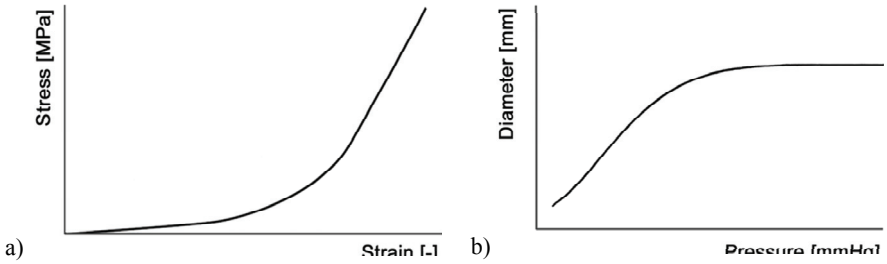

Fig. 2. Schematic non-linear load curves of a blood vessel wall:
(a) stress–strain curve in mechanical tests *in vitro*;
(b) diameter–pressure curve in tests *in vivo*

In the case of young and healthy people the behaviour of a vessel wall subjected to mechanical loads is determined mostly by the middle layer of the vessel and the adventitia. The tunica media of a vessel, built mainly of elastin fibres, collagen fibres, and smooth muscle cells, is responsible for the transfer of low mechanical loads acting on the wall, i.e. pressures existing under physiological work conditions of the vessel [51]. The adventitia, built mainly of collagen fibres, participates in load transfer at higher strain values by changing into a rigid tube that protects the vessel walls against excessive stretching and rupture [52]. On the other hand, the tunica intima of the aortic wall does not significantly affect its mechanical properties in the case of young and healthy individuals. However, with age, due to the development of atherosclerosis, the inner layer becomes thicker and the changes in its structure and composition, associated with the deposition of atheromatous plaques [53], significantly alter the mechanical properties of this layer [54].

Elastin fibres, collagen fibres, and smooth muscle cells are the basic structural components of blood vessel walls, determining their mechanical properties. Smooth muscle cells are responsible for active mechanical properties of the vessel wall because of their ability to contract and relax in response to mechanical and other stimuli [55]. On the other hand, elastin and collagen fibres are responsible for passive mechanical properties of the blood vessel wall [51], [56]. Elastic elastin fibres transfer loads at low load values (of pressures or forces) [57], whereas collagen fibres gradually take over the function of load transfer at increasingly higher values of the applied pressures or forces [58], [59]. The gradual inclusion of collagen fibres into the process of transfer of mechanical loads results in highly non-linear load curves, i.e. the relationship between stress and strain in the case of mechanical tests *in vitro* (figure 2a) and between diameter and pressure observed in tests *in vivo* (figure 2b) [56], [60], [61].

Atherosclerosis is one of the most common causes of death in developed and developing countries, but its etiology is still not fully known. The atherosclerotic process is characterized by cholesterol aggregation in the middle layer of a vessel. In the end stage of disease, wall calcification is observed, resulting in vessel stenosis and reduced blood flow. The atherosclerotic processes are mentioned as one of aortic aneurysm causative factors; they can also lead to arterial thrombosis (detached fragments of calcified plaque induce thrombus formation). The atheromatous plaque stability and risk of its detachment largely depend on its composition and structure [62]. Raman spectroscopy is used for assessing arterial lesions resulting from pathological processes and provides detailed information about e.g. the composition of an atheromatous plaque [5], [63]–[66].

The spectrum of healthy aorta is dominated by vibrational bands of its structural proteins – collagen and elastin (figure 1b, table 2) whose compositions change with disease progression, whereas the Raman spectrum of atherosclerotic tissue is dominated by the

Table 2. Major positions (in cm^{-1}) and tentative assignment of Raman bands of human aortic wall and calcium deposits [68].

ν [cm^{-1}]		Assignments*	
aortic wall	calcium deposits		
3600–3200		ν(OH), ν(NH)	proteins
2940	2935	$\nu(CH_2, CH_3)$	lipids and proteins
1664	1668	δ(NH), ν(CO)	amide I proteins
1450	1440	$\delta(CH_2, CH_3)$	lipids and proteins
1303	1304	$\delta(CH_2)$	lipids and proteins
1268	1270	δ(NH), ν(CN), ν(C–C)	amide III proteins
1257	1250		
	1071	$\nu_1(CO_3^{2-})/\nu_3(PO_4^{3-})$	HA
1004		$\Delta(C–C)_{ring}$	Phe
937		ν(C–C)	proteins
	960	$\nu_1(PO_4^{3-})$	HA
	591	$\nu_4(PO_4^{3-})$	HA
	450	$\nu_2(PO_4^{3-})$	HA
	430		

* Abbreviations: ν, stretching; δ, bending; Δ, breathing mode; HA, hydroxyapatite; Phe, phenylalanine.

lipid bands; increased intensities of the bands corresponding to cholesterol and its esters (880, 850, 720 and 700 cm^{-1}) are observed. The higher lipid contents are also confirmed by clearly broader bands of the CH_2 and CH_3 stretching and deformation vibrations as well as shifts of their maxima to lower wavenumbers. Moreover, in the spectra of a calcified atheromatous plaque (figure 1c), intense bands of the phosphate group vibrations are present, contrary to the spectra of healthy vessel walls [5], [56], [63], [66], [67].

The main calcium compound that occurs in its deposits in blood vessel walls is carbonate apatite of low crystallinity similar to that of bone or dentin mineral [69].

2.1.3. Bones

As shown in figure 1d, the Raman spectrum of bone reveals an intense band at around 960 cm^{-1} connected with the $\nu_1(PO_4)$ vibrations of hydroxyapatite ($Ca_{10}(PO)_46(OH)_2$) which constitutes 60–70% of the bone mineral mass. The $\nu_2(PO_4)$ and $\nu_4(PO_4)$ vibrations occur at 430 and 590 cm^{-1}, respectively. The presence of a band at around 1074 cm^{-1} in the Raman spectrum of bone means that within the hydroxyapatite lattice, the PO_4^{3-} groups are isomorphically replaced by CO_3^{2-} ions (5–8% wt% of the bone mineral mass) [65], which indicates the presence of type-B carbonate apatite typical of biological systems [70]. Broad bands within the 1200–1300 cm^{-1} (amide III) and 1620–1700 cm^{-1} (amide I) ranges are bands connected with vibrations of peptide bonds in proteins. Positions of the band maxima – at 1246 cm^{-1} for the amide III and at 1656 cm^{-1} for the amide I – are typical of collagen I which constitutes about 90% of the bone organic mass. The band at 1450 cm^{-1} is assigned to deformation vibrations of the CH_2 and CH_3 groups, whereas the band at 2935 cm^{-1} – to stretching vibrations [71]–[76].

Table 3. Major positions (in cm^{-1}) and tentative assignment of Raman bands of human bone [77]

ν [cm^{-1}]	Assignments*	
2935	$\nu(CH_2, CH_3)$	lipids and proteins
1656	δ(NH), ν(CO)	amide I proteins
1450	$\delta(CH_2, CH_3)$	lipids and proteins
1270	δ(NH), ν(CN), ν(C–C)	amide III proteins
1246		
1074	$\nu_1(CO_3^{2-})/(\nu_3(PO_4^{3-})$	HA
960	$\nu_1(PO_4^{3-})$	HA
590	$\nu_4(PO_4^{3-})$	HA
450	$\nu_2(PO_4^{3-})$	HA
430		

* Abbreviations: ν, stretching; δ, bending mode; HA, hydroxyapatite.

The hydroxyapatite content in bone tissue and its composition depend on the bone type, age, presence of disease processes, nutritional habits and physical activity of a person. The bone structure determines its biomechanical properties. Such parameters as the degree of tissue mineralization, hydroxyapatite crystallinity level and the presence of

substitutions within the crystal lattice can be determined by means of Raman and infrared spectroscopy [74], [76], [78]–[84]. The degree of bone mineralization can be determined from a Raman spectrum through calculating the ratio of integral intensities of the $\nu_1(PO_4)$ vibrational band (~960 cm^{-1}) and the amide I band (~1656 cm^{-1}). Crystallinity levels of bone samples can be compared when the half-width of $\nu_1(PO_4)$ band is determined. The degree of substitution of the phosphate groups for the CO_3^{2-} groups in the hydroxyapatite lattice is calculated as a ratio of the $\nu_3(PO_4)$, $\nu_1(CO_3)$ (~1071 cm^{-1}) integral intensities to the $\nu_1(PO_4)$ (~961 cm^{-1}) band intensity [75], [78], [81].

2.1.4. Studies of mechanical properties with the use of Raman spectroscopy

Mechanical properties of tissues are also influenced by the orientation of collagen and elastin fibres. Identification of protein fibre orientation is possible by means of Raman spectroscopy. In view of the fact that the intensities of certain bands in the Raman spectrum depend on the orientation of excitation beam: ν_1PO_4 stretching vibration is strongest parallel to the axis of the fibre. The scattering of amide I bands is more intense in the perpendicular direction to the fibre axis; it was demonstrated that 90% type I collagen fibrils is locally oriented predominantly parallel to each other in long bones [72], [78]. Based on optical anisotropy of collagen fibres, JANKO et al. [85] studied the distribution of collagen fibres in human skin. MASIC et al. applied Polarized Raman Spectroscopy for observations of stress-induced changes of collagen orientation in tendon [86].

Raman spectroscopic techniques may also be utilized for describing conformational changes in proteins due to stress. Studies on polymers and natural fibres, including collagen [10], [38], [87]–[90], revealed that stress applied to chemical bonds leads to changes in interatomic distances and consequently, due to the inharmonicity of the vibrational energy, it shifts positions of the bands. First of all, the amide bands and the bands of C–C stretching vibrations change their positions in the Raman spectrum with increasing protein deformation. For spider silk, SIRICHAISIT et al. [88] observed an approximately linear dependence between the ν(C–C) band position (in the Raman spectrum of non-stretched structure: 1095 cm^{-1}) and the fibre deformation value. The studies conducted by WANG [38] revealed that for the collagen spectrum, vibrations (822, 1166, 1418, 1443 and 1460 cm^{-1}) are shifted to lower frequencies, whereas vibrations of 879, 952, 1392 and 1684 cm^{-1} are shifted to higher wavenumbers. The observed vibration frequency changes are fairly significant, e.g., about 2.5 cm^{-1} with 13% stress for the ν(C–C) (822 cm^{-1}) vibration. The decrease of the half-width of this band is approximately linear, which is related to straightening of the molecular kinks during collagen fibre stretching.

Analogical studies were conducted for more complex structures, i.e. tissues. A combination of Raman spectroscopy and single-axis stretch tests allowed for a detailed description of the mechanism related to load transfer by collagen and elastin in tissues containing these proteins, i.a. tendon, ligaments, aortic wall and skin [35], [37], [40], [56], [91].

2.2. DNA

Raman spectrum of DNA can be divided into characteristic spectral regions (figure 3). The first one is the broad band centered at 1668 cm^{-1} assigned to coupled C=O stretching and N–H deformation modes of dT, dG and dC. This band is sensitive to denaturation process. In the next interval 1600–1200 cm^{-1} there are located bands associated to purine and pyrimidine ring vibrations. The bands in this region are sensitive to conformational transition and melting process. In addition, they exhibit perturbation upon metal binding at ring sites. It was observed that these bands are sensitive indicators of electronic structures of the ring. The PO_2^- band centered near 1092 cm^{-1} is susceptible to changes in the electrostatic environment of the phosphate groups. The bands in the next range 1100–800 cm^{-1} are responsive to backbone geometry and secondary structure. The region 800–600 cm^{-1} includes bands that are sensitive to nucleoside conformation. The Raman line near 750 cm^{-1} is assigned to C2′-endo/anti conformers of thymidine. The band near 727 cm^{-1} is associated to vibrations of adenine residue. In the interval 685–620 cm^{-1} there are placed diagnostic bands of sugar pucker and glycosyl torsion of dG residues [92]–[94]. In table 4, major Raman bands and their assignments for DNA are presented. Raman spectra of nucleic acids in aqueous solution do not depend on the strong water absorption. In this method water bands do not overlap bands of nucleic acids. Thus, Raman spectroscopy can be successfully used to study solids and aqueous solutions of DNA. This method similar to the IR spectroscopy provides important information about the structure of DNA in different environmental conditions.

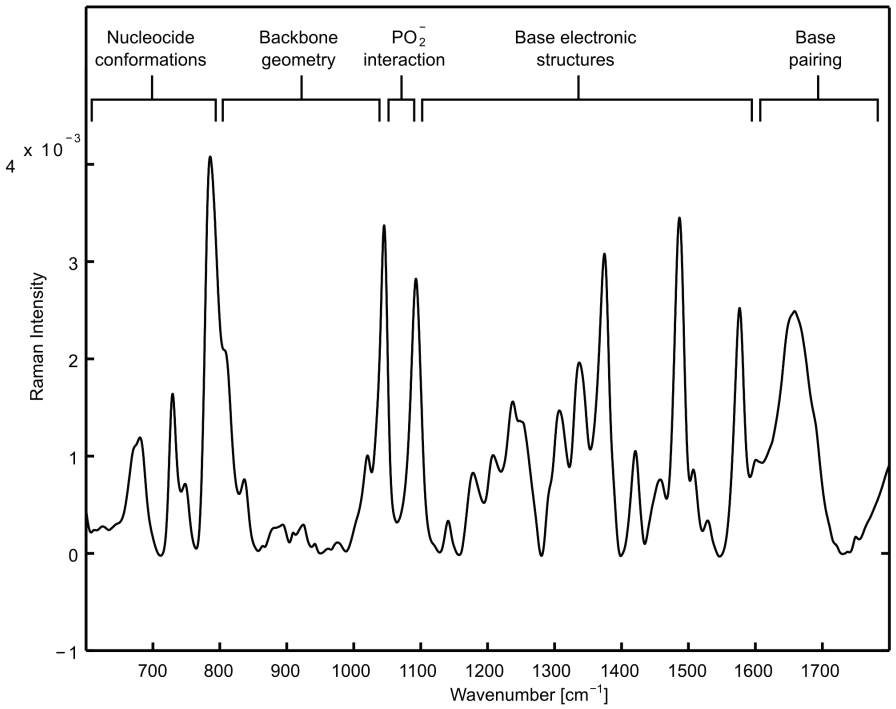

Fig. 3. Raman spectrum of herring sperm DNA in the interval 600–1700 cm^{-1}. Labels identify bands assigned to specific base, sugar and phosphate vibrations

Table 4. Major positions (in cm^{-1}) and tentative assignment of Raman bands of B-DNA

ν [cm^{-1}]	Assignments*
1688	ν(C=O), $\delta(NH_2)$ of dT, dG, dC
1610	dC
1578	dG, dA
1534	dC
1511	dA, dC
1489	dG, dA
1421	d purine/syn
1376	dT, dA, dG
1339	dA, dG
1320	dG
1304	dA
1292	dC
1257	dC, dA
1238	dT
1218	dT
1186	dT, dC
1142	ν(C–C)
1094	$\nu_s(PO_2^-)$
1054	ν(C–O)
895	d
835	ν(O–P–O)
781	dC
750	dT
729	dA
682	G C2′-endo/anti

* Abbreviations: ν, stretching; δ, in-plane bending; *s*, symmetrical; dA, deoxyadenosine; dC, deoxycytidine; dG, deoxyguanosine; dT, thymidine; d, deoxyribose.

2.2.1. DNA denaturation

Raman spectroscopy is an excellent analytical tool for studying DNA denaturation processes [95], [96]. Denaturation of this macromolecule occurs in two stages: the premelting stage and the melting stage. The first stage refers to structural changes in DNA that are induced before strand separation begins, i.e. before the melting temperature $T_{m.}$ is reached. Melting occurs after reaching the melting temperature, at which hydrogen bonds between the bases are destroyed and separation of the DNA strands occurs. Each of those stages can be successfully studied by using Raman spectroscopy. Contrary to infrared spectroscopy characterized by very strong IR absorption by water, in the Raman spectroscopy, scattering of radiation by water is weak. Therefore, this method allows for detailed analysis of bands corresponding to base vibrations and studying melting process of DNA solution. In table 5, structural changes in poly(dA–dT)*poly(dA–dT) during premelting and melting processes are presented.

In [95] authors have reported that during denaturation of calf-thymus DNA, the bands corresponding to deoxyribose and deoxyribose-phosphate vibrations, located in the range 828–1047 cm^{-1} showed reduction of intensities with increasing temperature. These backbone vibrations indicate of changes observed in

Table 5. Major positions (in cm^{-1}) and tentative assignment of Raman bands of poly (dA–dT)*poly(dA–dT) observed during premelting and melting transition. Plus (or minus) sign indicates that the band has gained (or lost) appreciable intensity as a result of DNA melting

Premelting			Melting		
ν [cm^{-1}]	Changes of spectral parameters	Assignments*	ν [cm^{-1}]	Changes of spectral parameters	Assignments*
670	660	C2'-endo dA→ C3'-endo dA	727	+727	Unstacking of adenine
731	724	Change of adenine hydrogen bonding	792	790	Change of phospho-diester conformation
752	742	C2'-endo dT→ C3'-endo dT	840	878	Change of phospho-diester conformation
792	790	Change of phospho-diester conformation	924	–924	Change of deoxyribose conformation
840	878	Change of phospho-diester conformation	970	–970	Change of deoxyribose conformation
1000–1082	+1000–1082	Change of deoxyribose conformation	1000–1082	+1000–1082	Change of deoxyribose conformation
1242	–1242	Change of thymine hydrogen bonding	1182	+1182	Unpairing of thymine
1262	–1262	Change of thymine hydrogen bonding	1200	+1200	Unpairing of thymine
1345	1330	C2'-endo dA→ C3'-endo dA	1237	+1237	Unstacking of thymine
1379	1365	Change of thymine hydrogen bonding	1309	+1309	Unstacking of adenine
1420–1465	–1420–1465	Change of deoxyribose conformation	1345	1330	C2'-endo dA→ C3'-endo dA
1516	1502	Change of adenine hydrogen bonding	1369	+1369	Unstacking of adenine and thymine
1579	1571	Change of adenine hydrogen bonding	1413	+1413	Unstacking of adenine
1640	+1640	Change of thymine hydrogen bonding	1420–1465	–1420–1465	Change of deoxyribose conformation
1688	+1688	Change of thymine hydrogen bonding	1480	+1480	Unstacking of adenine
			1516	1502	Change of adenine hydrogen bonding
			1581	+1581	Unstacking of adenine
			1663	+1663	Unstacking and unpairing of thymine
			1688	+1688	Unstacking and unpairing of thymine

the backbone conformation upon melting. However, no changes of these vibrations were observed before reaching T_m, which means that the sugar-phosphate backbone geometry was intact. Moreover, the decrease in intensity and broadening of the band (studies conducted in D_2O) above the melting temperature T_m were also observed for the 1047 cm^{-1} band assigned to the C–O stretching vibrations of deoxyribose. The analysis of this band showed no changes during premelting, which is the evidence that this fragment of the backbone is intact before reaching the melting temperature. Also, Raman spectra analysis showed that bands located at 785 and 1091 cm^{-1}, assigned respectively to the O–P–O of diester symmetric stretch and the PO_2^- symmetric stretching vibrations, did not change with increasing temperature.

2.2.2. DNA and metals

Raman spectroscopy was also used to study interactions between DNA molecules and metal ions. As shown in many experiments [97]–[100], alkaline-earth metal ions stabilize DNA, whereas transition metal

ions destabilize this macromolecule. Stabilizing effects of alkaline-earth metal ions are related to direct binding of these ions to DNA phosphates, resulting in reduced repulsions between complementary DNA strands. There is the evidence that alkaline-earth metal ions especially Ca^{2+} and Mg^{2+} primarily interact with negatively-charged phosphate groups but also show a weak interaction with the DNA bases [101]. It means that ions of this group can also bind to bases or at least indirectly influence them, e.g. they can enhance stacking interactions between the bases through reduction of electrostatic repulsions between adjacent DNA stands. Transition metal ions, in turn, show a high binding affinity to nitrogenous bases (the highest to the N7 atom of guanine), resulting in destabilization of DNA molecule. Moreover, divalent ions might cause DNA aggregation at higher temperatures [101]. In the studies applying the Raman spectroscopy it was shown that at temperatures below T_m, alkaline-earth metal ions slightly affected the DNA structure compared to the transition metal ions. Disorders caused by Sr^{2+} ions are very weak, while Ba^{2+}, Mg^{2+} and Ca^{2+} cations disrupt the structure of DNA in a more distinct manner [94]. Binding of metal ions to phosphates is manifested by decrease in intensity of the band at 1093 cm^{-1} assigned to PO_2^- symmetric stretching vibrations. The reduced intensity of this band is probably caused by the covalent bonding of the oxygen atom of a phosphate group and metal ion (–P(=O)–O–metal). Moreover, the band intensity decrease is proportional to the amount of metal ions that will bind to the phosphate group [101]. Binding of metal ions to bases can be demonstrated by changes within the bands located within the 1200–1500 cm^{-1} range. The guanine marker, located at 1489 cm^{-1} in the Raman spectrum of DNA with no metal additive, is shifted to lower frequencies after metal ion binding. It was also observed that the band at 1257 cm^{-1}, assigned to the dC vibrations, showed increase in intensity after alkaline-earth metal ion binding. This behavior may indicate that these ions cause a slight weakening of stacking interactions of cytosine [94]. Significant changes can be observed within the bands located at 1208 and 1218 cm^{-1} assigned to adenine and thymine vibrations, respectively. When a magnesium ion binds to DNA, both lines are linked into one band at 1228 cm^{-1}. These changes may suggest a partial separation of base pairs [103]. Greater disturbances are seen within the carbonyl vibration region at 1668 cm^{-1}. It is suggested that these ions induce modifications of hydrogen bonds between the bases and disrupt the DNA-bound water structure [94].

As shown in studies conducted by DUGUID et al. [94], transition metal ions evidently modify the B-DNA structure. Drastic changes occur within bands sensitive to base paring. The band at 1668 cm^{-1}, assigned to the coupled C=O stretching and N–H deformation vibrations, is shifted to 1656 cm^{-1} after transition metal ion binding. Such a large shift suggests disruption of hydrogen bonds between the bases due to interactions of the exocyclic dG groups and NH_2 dA groups with transition metals. Moreover, disruption of the stacking interactions between nucleic bases is observed. Changes in intensity of bands sensitive to stacking interaction, located at 1240, 1304, 1337, 1376 and 1578 cm^{-1} indicate DNA structure disruption. Furthermore, strong hyperchromism of these bands, indicating that the stacking interactions between the bases have been destroyed by the transition metal ions, is observed. Some transition metal ions, particularly Cu^{2+}, indicate the possibility of interaction with the PO_2^- groups. The decrease in the intensity of the band at 1092 cm^{-1} in the Raman spectrum of the Cu-DNA complex proves the existence of such interactions.

Analysis of the Raman spectra of DNA-metal complexes showed that some ions cause DNA aggregation at elevated temperatures. In the study [104], the effects of alkaline-earth metal ions on the DNA melting process were investigated. During the denaturation intensity changes of bands located at 1335 cm^{-1} and 1374 cm^{-1}, assigned to the dA, dG and dT, dA, dG vibrations, respectively, were observed. The behavior of these peaks in Raman spectra was correlated with the ability to aggregate DNA-metal complexes at elevated temperatures. Analysis of I_{1335}/I_{1374} ratio showed that the aggregation occurs if the value is > 1. It was also observed that higher values of this ratio correspond to lower melting temperatures of DNA-metal complexes and lower aggregation temperatures. The Sr-DNA and Ba-DNA complexes show the ratios $I_{1335}/I_{1374} < 1$, which means they are not capable for forming aggregates. On the other hand, Ni- and Cd-DNA complexes ($I_{1335}/I_{1374} > 1$) undergo strong aggregation and have low Tm values. Intermediate values, i.e., $I_{1335}/I_{1374} \approx 1$, were observed for Mg-, Ca- and Mn-DNA complexes. Raman spectroscopy studies combined with DSC analysis allowed to propose a mechanism describing aggregation process initiated by metal ions. The authors present two models describing this process. The first model postulate that the aggregation probably occurs through the crosslinks of partly melted DNA fragments, whereas the second shows that the duplex remains intact.

2.2.3. The effects of pH

Raman spectroscopy was used to monitor the DNA melting process induced by pH changes [105]. Acid denaturation caused by reducing pH value to 2 occurs in two consecutive stages. The first stage refers to adenine and guanine protonation (pH 4.1) as well as C-DNA formation. The Raman analysis shows that protonation of cytosine occurs at pH of 5.54–4.09 and is manifested by reduced intensity of the band located at 1252 cm^{-1}. Adenine protonation takes place within the same pH range. Binding of H^+ ions to adenine leads to intensity changes of the bands located at 1335, 1373 and 1476 cm^{-1}. Reduction of pH values to <3 cause the decrease in intensity of the band located at 1476 cm^{-1}, which can be explained by H^+ ion binding to N(7) of guanine. Changes of pH values also affect the region of phosphate group vibrations. In the Raman spectrum recorded for pH = 4.09, a disappearance of the 835 cm^{-1} band corresponding to the B-DNA conformation and the presence of a new band at 879 cm^{-1} were reported. This band can be assigned to C-DNA. During the second stage of acid denaturation, true macromolecule degradation was observed. The stacking interactions of adenine residues are destroyed within the range of adenine protonation. It is manifested by changes in the intensity of the band located at 721 cm^{-1}. The stacking interactions of cytosine can be monitored through observation of the 723 cm^{-1} band whose intensity does not change due to protonation of the base. When pH reaches 3.3, the Raman spectrum shows a loss of the stacking interactions for adenine, thymine and cytosine bases.

Base denaturation of DNA molecule, contrary to acid denaturation, occurs within a very limited pH range. At pH = 11, intensity changes of the bands located at 1252 cm^{-1} (partial contribution of thymine) and 1476 cm^{-1} (partial contribution of guanine) are observed. These changes prove that H^+ ions are removed from the N(3) of thymine and N(1) of guanine. Deprotonation of guanine bases occurs at lower pH values than those observed for thymine. The lines located at 721 and 783 cm^{-1} are diagnostic bands, which prove the existence of stacking interactions for adenine and cytosine bases. The increase in intensities of these bands denotes a loss of the stacking interactions. Thus, base denaturation of DNA is initiated by deprotonation of guanine, followed by thymine deprotonation. The consequence of these processes is a loss of the stacking interactions.

Acknowledgements

This publication is part of the Project „WroVasc – Integrated Cardiovascular Centre", co-financed by the European Regional Development Fund, within Innovative Economy Operational Program, 2007–2013 realized in Regional Specialist Hospital, Research and Development Center in Wroclaw. "European Funds – for the development of innovative economy".

References

[1] OLSZTYŃSKA-JANUS S., SZYMBORSKA-MAŁEK K., GĄSIOR-GŁOGOWSKA M., WALSKI T., KOMOROWSKA M., WITKIEWICZ W., PEZOWICZ C. KOBIELARZ M., SZOTEK S., *Spectroscopic techniques in the study of human tissues and their components*. Part I: *IR spectroscopy*, Acta of Bioengineering and Biomechanics, 2012, 14, 101–115.

[2] PARKER F.S., *Application of infrared Raman and resonance Raman spectroscopy in biochemistry*, Plenum Press, New York, 1983.

[3] SCHRADER B., KELLER S., LÖCHTE T., FENDEL. S., MOORE D.S., SIMON A., SAWATZKI J., *NIR FT Raman spectroscopy in medical diagnosis*, J. Mol. Struct., 1995, 348, 293–296.

[4] SCHRADER B., DIPPEL B., ERB I., KELLER S., LÖCHTE T., SCHULZ H., TATSCH E., WESSEL S., *NIR Raman spectroscopy in medicine and biology: results and aspects*, J. Mol. Struct., 1999, 480–481, 21–32.

[5] MANOHARAN R., WANG Y., FELD M.S., *Histochemical analysis of biological tissues using Raman spectroscopy*, Spectrochim. Acta, 1996, 52, 215–249.

[6] SHIM M.G., WILSON B.C., *Development of an In Vivo Raman spectroscopic system for diagnostic applications*, J. Raman Spectrosc., 1997, 28, 131–142.

[7] PAPPAS D., SMITH B.W., WINEFORDNER J.D., *Raman spectroscopy in bioanalysis*, Talanta, 2000, 51, 131–144.

[8] LYNG F.M., FAOLÁIN E.Ò., CONROY J., MEADE A.D., KNIEF P., DUFFY B., HUNTER M.B., BYRNE J.M., KELEHAN P., BYRNE H.J., *Vibrational spectroscopy for cervical cancer pathology from biochemical analysis to diagnostic tool*, Exp. Mol. Pathol., 2007, 82, 121–129.

[9] SALZER R., SIESLER H.W., *Infrared and Raman spectroscopic imaging*, Wiley-VCH Verlag GmbH & Co KgaA, Weinheim, Germany, 2009.

[10] AMER M.S., *Raman Spectroscopy for Soft Matter Applications*, John Wiley & Sons Inc., Hoboken, New Jersey, 2009.

[11] DOWNES A., ELFICK A., *Raman spectroscopy and related techniques in biomedicine*, Sensor, 2010, 10, 1871–1889.

[12] MOVASAGHI Z., REHMAN S., REHMAN U.I., *Raman spectroscopy of biological tissues*, Appl. Spectrosc. Rev., 2007, 42, 5, 493–541.

[13] AGACHE P., HUMBERT P., *Measuring the skin*, Springer, Verlag, Berlin, Germany, 2004.

[14] GEERLIGS M., *Skin layer mechanics*, PhD Thesis, TU Eindhoven, 2010.

[15] SCOTT D.W., MILLER W.H., GRIFFIN C.E., *Muller & Kirk's Small Animal Dermatology*, W.B. Saunders Company, Philadelphia, 2001.

[16] FARAGE M.A., MILLER K.W., MAIBACH H.I., *Textbook of Aging Skin*, Springer, 2010.

[17] SILVER F.H., *Mechanosensing and Mechanochemical Transduction in Extracellular Matrix Biological Chemical Engineering and Physiological Aspects*, Springer, New York, 2006.

[18] ROSENBLOOM J., ABRAMS W.R., MECHAM R., *Extracellular matrix 4: the elastic fiber*, Faseb. J., 1993, 7, 13, 1208–1218.

[19] LANGER K., *On the anatomy and physiology of the skin*, British J. Plast. Surg., 1978, 17, 31, 93-106

[20] ARUMUGAM V., NARESH M.D., SANJEEVI R., *Effect of strain rate on the fracture behavior of skin*, J. Biosci., 1994, 19, 307–313.

[21] SZOTEK S., BĘDZIŃSKI R., KOBIELARZ M., GĄSIOR-GŁOGOWSKA M., KOMOROWSKA M., MAKSYMOWICZ K., HANUZA J., HERMANOWICZ K., *Human skin properties determined by mechanical tests and Raman spectroscopy*, Eng. Biomater., 2009, 89–91, 208–210.

[22] NÍ ANNAIDH A., BRUYÈRE K., DESTRADE M., GILCHRIST M.D., OTTÉNIO M., *Characterization of the anisotropic mechanical properties of excised human skin*, J. Mech. Behav. Biomed., 2011, (doi:10.1016/j.jmbbm.2011.08.016)

[23] GNIADECKA M., NIELSEN O.F., CHRISTENSEN D.H., WULF H.C., *Structure of water proteins and lipids in intact human skin hair and nail*, J. Invest. Dermatol., 1998, 110, 393–398.

[24] EDWARDS H.G.M., GNIADECKA M., PETERSEN S., HANSEN J.P.H., NIELSEN O.F., CHRISTENSEN D.H., WULF H.C., *NIR-FT Raman spectroscopy as a diagnostic probe for mummified skin and nails*, Vib. Spectrosc., 2002, 28, 3–15.

[25] KNUDSEN. L., JOHANSSON C.K., PHILIPSEN P.A., GNIADECKA M., WULF H.C., *Natural variations and reproducibility of in vivo near-infrared Fourier transform Raman spectroscopy of normal human skin*, J. Raman Spectrosc., 2002, 33, 574–579.

[26] AKHTAR W., EDWARDS H.G.M., *Fourier-transform Raman spectroscopy of mammalian and avian keratotic biopolymers*, Spectrochim. Acta A, 1997, 53, 81–90.

[27] GREVE T.M., ANDERSEN K.B., NIELSEN O.F., *ATR-FTIR FT-NIR and near-FT-Raman spectroscopic studies of molecular composition in human skin in vivo and pig ear skin in vitro*, Spectrosc., 2008, 22, 437–457.

[28] EDWARDS H.G.M., WILLIAMS A.C., BARRY B.W., *Potential Applications of FT-Raman Spectroscopy for Dermatological Diagnostics*, J. Mol. Struct., 1995, 347, 379–358.

[29] SHIM M.G., WILSON B.C., *Development of an In Vivo Raman Spectroscopic System for Diagnostic Applications*, J. Raman Spectrosc., 1997, 28, 131–142.

[30] ANIGBOGU A.N.C., WILLIAMS A.C., BARRY B.W., EDWARDS H.G.M., *Fourier transform Raman spectroscopy of interactions between the penetration enhancer dimethyl sulfoxide and human stratum corneum*, Int. J. Pharm., 1995, 125, 265–282.

[31] DONG R., YAN X., PANG X., LIU S., *Temperature-dependent Raman spectra of collagen and DNA*, Spectrochim. Acta A, 2004, 60, 557–561.

[32] LYNG F.M., FAOLAIN E.O., CONROY J., MEADE A.D., KNIEF P., DUFFY B., HUNTER M.B., BYRNE J.M., KELEHAN P., BYRNE H.J., *Vibrational spectroscopy for cervical cancer pathology from biochemical analysis to diagnostic tool*, Exp. Mol. Pathol., 2007, 82, 121–129.

[33] MANOHARAN R., WANG Y., FELD M.S., *Histochemical analysis of biological tissues using Raman spectroscopy*, Spectrochim. Acta A, 1996, 52, 215–249.

[34] CHENG W.T., LIU M.T., LIU H.N., LIN S.Y., *Micro-Raman spectroscopy used to identify and grade human skin pilomatrixoma*, Mircosc. Res. Tech., 2005, 68, 2, 75–79.

[35] PENTEADO S.G., MENESES C.S., DE OLIVEIRA LOBO A., MARTIN A.A., DA SILVA MARTINHO H., *Diagnosis of rotator cuff lesions by FT-Raman spectroscopy: a biochemical study*, presented at SPEC 2006 Shedding Light on Disease: Optical Diagnosis for the New Millenium 4th International Conference, 20–24th May 2006, Heidelberg, Germany.

[36] POŁOMSKA M., KUBISZ L., KALAWSKI R., OSZKINIS G., FILIPIAK R., MAZUREK A., *Fourier Transform Near Infrared Raman spectroscopy in studies on connective tissue*, Acta Phys. Pol. A, 2010, 118, 136–140.

[37] GĄSIOR-GŁOGOWSKA M., KOMOROWSKA M., HANUZA J., PTAK M., KOBIELARZ M., *Structural alteration of collagen fibres – spectroscopic and mechanical studies*, Acta Bioeng. Biomech., 2010, 12, 4, 25–32.

[38] WANG Y.-N., GALIOTIS C., BADER D.L., *Determination of molecular changes in soft tissues under strain using laser Raman microscopy*, J. Biomech., 2000, 33, 4, 483–486.

[39] COLOMBAN PH., DINH H.M., RIAND J., PRINSLOO L.C., MAUCHAMP B., *Nanomechanics of single silkworm and spider fibres: a Raman and micro-mechanical in situ study of the conformation change with stress*, J. Raman Spectrosc., 2008, 39, 1749–1764.

[40] GĄSIOR-GŁOGOWSKA M., KOMOROWSKA M., HANUZA J., MĄCZKA M., ZAJĄC A., BĘDZIŃSKI R., KOBIELARZ M., MAKSYMOWICZ K., KUROPKA P., SZOTEK S., *FT-Raman spectroscopic study of human skin subjected to uniaxial stress*, in preparation.

[41] FENDEL S., SCHRADER B., *Investigation of skin and skin lesions by NIR-FT-Raman spectroscopy*, Fresenius J. Anal. Chem., 1998, 360, 609–613.

[42] GNIEDECKA M., PHILIPSEN P.A., SIGURDSSON S., NIELSEN O.F., CHRISTENSEN D.H., HERCEGOVA J., ROSSEN K., THOMSEN H.K., GNIADECKI R., HANSEN L.K., WULF H.CH., *Melanoma diagnosis by Raman spectroscopy and neural network: structure alterations in proteins and lipids in intact cancer tissue*, J. Invest. Dermatol., 2004, 122, 443–449.

[43] SIGURDSSON S., PHILIPSEN P.A., HANSEN L.K., LARSEN J., GNIADECKA M., WULF H.C., *Detection of Skin Cancer by Classification of Raman Spectra*, IEEE T Bio-Med. Eng., 2004, 51, 10, 1784–1793.

[44] ZENG H., LUI H., MCLEAN D.I., *Skin cancer detection using in vivo Raman spectroscopy*, 2011, (DOI: 10.1117/2.1201104.003705).

[45] GNIADECKA M., NIELSEN O.F., WULF H.C., *Water content and structure in malignant and benign skin tumours*, J. Mol. Struct., 2003, 661–662, 405–410.

[46] NAKAGAWA N., MATSUMOTO M., SAKAI S., *In vivo measurement of the water content in the dermis by confocal Raman spectroscopy*, Skin Res. Technol., 2010, 16, 137–141.

[47] EGAWA M., HIRAO T., TAKAHASHI M., *In vivo estimation of stratum corneum thickness from water concentration profiles obtained with Raman spectroscopy*, Acta Derm. Venereol., 2007, 87, 1, 4–8.

[48] LIN S.Y., LI M.J., CHENG W.T., *FT-IR and Raman vibrational microspectroscopies used for spectral biodiagnosis of human tissues*, Spectroscopy, 2007, 21, 1–3.

[49] KOBIELARZ M., MAKSYMOWICZ K., KALETA K., KUROPKA P., MARYCZ K., BĘDZIŃSKI R., *Histological and ultrastructural evaluation of the walls of abdominal aortic aneurysms*, J. Eng. Biomater., 2010, 13, 83–87.

[50] THOMPSON R., GERAGHTY P., LEE J., *Abdominal aortic aneurysms: basic mechanisms and clinical implications*, Curr. Prob. Surg., 2002, 39, 93–232.

[51] XIE J., ZHOU J., FUNG Y., *Bending of blood vessel wall: stress-strain laws of the intima-media and adventitia layers*, J. Biomech. Eng., 1995, 117, 136–145.

[52] SCHULZE-BAUER C., REGITINIG P., HOLZAPFEL G., *Mechanics of the human femoral adventitia including high-pressure re-*

sponse, Am. J. Physiol. Heart Circ. Physiol., 2002, 282, 6, H2427-H2440.

[53] KOT M., KOBIELARZ M., MAKSYMOWICZ K., *Assessment of mechanical properties of arterial calcium deposition*, T. Famena, 2011, 35, 49–56.

[54] VITO R., DIXON S., *Blood vessel constitutive models – 1995–2002*, Ann. Rev. Bio. Eng., 2003, 5, 413–439.

[55] BANK A., KAISER D., *Smooth muscle relaxation-effect on arterial compliance distensibility elastic modulus and pulse wave velocity*, Am. J. Hypertens., 1998, 32, 356–359.

[56] HANUZA J., MĄCZKA M., GĄSIOR-GŁOGOWSKA M., KOMOROWSKA M., BĘDZIŃSKI R., SZOTEK S., MAKSYMOWICZ K., HERMANOWICZ K., *FT-Raman spectroscopic study of thoracic aortic wall subjected to uniaxial stress*, J. Raman Spectrosc., 2009, 40, 1163–1169.

[57] CARMO M., COLOMBO L., BRUNO A., CORSI F., RONCORONI L., CUTTIN M., RADICE F., MUSSINI E., SETTEMBRINI P., *Alteration of elastin collagen and their cross-links in abdominal aortic aneurysms*, Eur. J. Vasc. Endovas., 2002, 23, 543–549.

[58] ROBICSEK F., THUBRIKAR M., FOKIN A., *Cause of degenerative disease of the trileaflet aortic valve: review of subject and presentation of a new theory*, Ann. Thor. Surg., 2002, 73, 1346–1354.

[59] KOBIELARZ M., MAKSYMOWICZ K., BĘDZIŃSKI R., *Elastin and collagen fibres alterations for abdominal aortic aneurysms population with constant maximum diameter size*, J. Eng. Biomater., 2011, 14, 2–6.

[60] SONESSON B., LANNE T., VERNERSSON E., HANSEN F., *Sex difference in the mechanical properties of the abdominal aorta in human beings*, J. Vasc. Surg., 1994, 20, 959–969.

[61] VAN BAVEL E., SIERSMA P., SPAAN J., *Elasticity of passive blood vessels: a new concept*, Am. J. Physiol-Heart, 2003, 285, H1986–H2000.

[62] WILLERSON J.T., CAMPBELL W.B., WINNIFORD M.D., *Conversion from chronic to acute coronary artery disease: speculation regarding mechanism*, Am. J. Cardiol., 1984, 54, 1349–1354.

[63] RÖMER T.J., BRENNAN III J.F., BAKKER SCHUT T.C., WOLTHUIS R., VAN DEN HOOGEN R.C.M., EMEIS J.J., VAN DER LAARSE A., BRUSCHKE A.V., PUPPELS G.J., *Raman spectroscopy for quantifying cholesterol in intact coronary artery wall*, Atherosclerosis, 1998, 141, 117–124.

[64] VAN DEL POLL S.W.E., ROMER T.J., PUPPELS G., VAN DER LAARSE A., *Raman spectroscopy of atherosclerosis*., J. Cardiovasc. Risk, 2002, 9, 255–261.

[65] PENEL G., CAU E., DELFOSSE C., REY CH., HARDOUIN P., JEANFILS J., DELECOURT CH., LEMAITRE J., LEROY G., *Raman Microspectrometry Studies of Calcified Tissues and Related Biomaterials*. *Raman Studies of Calcium Phosphate Biomaterials*, Dent. Med. Probl., 2003, 40, 1, 37–43.

[66] DE PAULA A.R., SATHAIAH S., *Raman spectroscopy for diagnosis of atherosclerosis: a rapid analysis using neural networks*, Med. Eng. Phys., 2005, 27, 237–244.

[67] BUSCHMAN H.P., MOTZ J.T., DEINUM G., ROMER T.J., FITZMAURICE M., KRAMER J.R., VAN DER LAARSE A., BRUSCHKE A.V., FELD M.S., *Diagnosis of human coronary atherosclerosis by morphology-based Raman spectroscopy*, Cardiovasc. Pathol., 2001, 10, 59–68.

[68] GĄSIOR-GŁOGOWSKA M., MISIAK H., OLSZTYŃSKA-JANUS S., KOMOROWSKA M., HANUZA J., MAKSYMOWICZ K., KOBIELARZ M., *NIR-FT Raman and ATR FT-IR spectroscopic characterization of human atherosclerotic plaques*, in preparation.

[69] LEGEROS R.Z., *Formation and transformation of calcium phosphates: relevance to vascular calcification*, Kardiol., 2001, 90, Suppl 3 III/116–III/124.

[70] ELLIOTT J., HOLCOMB D., YOUNG R., *Infrared determination of the degree of substitution of hydroxyl by carbonate ions in human dental enamel*, Calcif. Tissue Int., 1985, 37, 372–375.

[71] SMITH R., REHMAN I., *Fourier transform Raman spectroscopic studies of human bone*. J. Mater. Sci: Mater. Med., 1995, 5, 775–778.

[72] DE CARMEJANE O., MORRIS M.D., DAVIS M.K., STIXRUDE L., TECKLENBURG M., RAJACHAR R.M., KOHN D.H., *Bone Chemical Structure Response to Mechanical Stress Studied by High Pressure Raman Spectroscopy*, Calcif. Tissue. Int., 2005, 76, 207–213.

[73] PENEL G., LEROY G., REY C., BRES E., *MicroRaman Spectral Study of the PO4 and CO3 Vibrational Modes in Synthetic and Biological Apatites*, Calcif. Tissue. Int., 1998, 63, 475–481.

[74] PENEL G., DELFOSSE C., DESCAMPS M., LEROY G., *Composition of bone and apatitic biomaterials as revealed by intravital Raman microspectroscopy*, Bone, 2005, 36, 893–901.

[75] GAMSJAEGER S., MASIC A., ROSCHGER P., KAZANCI M., DUNLOP J.W.C., KLAUSHOFER K., PASCHALIS E.P., FRATZL P., *Cortical bone composition and orientation as a function of animal and tissue age in mice by Raman spectroscopy*, Bone, 2010, 47, 392–399.

[76] KOZIELSKI M., BUCHWALD T., SZYBOWICZ M., BŁASZCZAK Z., PIORTOWSKI A., CIESIELCZYK B., *Determination of composition and structure of spongy bone tissue in human head of femur by Raman spectral mapping*, J. Mater. Sci. Mater. Med., 2011, 22, 1653–1661.

[77] NIKODEM A., DOBRZAŃSKI Z., *Influence of calcium content in feed phosphate on mechanical properties of bone tissue*, Eng. Biomater., 2011, 14, 109–111, 78–80.

[78] KAZANCI M., ROSCHGER P., PASCHALIS E.P., KLAUSHOFER K., FRATZL P., *Bone osteonal tissues by Raman spectral mapping: orientation-composition*, J. Struct. Biol., 2006, 156, 489–496.

[79] TERMINE J.D., POSNER A.S., *Infra-red determination of the percentage of crystallinity in apatitic calcium phosphates*, Nature, 1966, 211, 268–270.

[80] CARDEN A., MORRIS M.D., *Application of vibrational spectroscopy to the study of mineralized tissues (review)*, J. Biomed. Opt., 2000, 5, 259–268.

[81] AKKUS O., ADAR F., SCHAFFLER M.B., *Age-related changes in physicochemical properties of mineral crystals are related to impaired mechanical function of cortical bone*, Bone, 2004, 34, 443–453.

[82] SAHAR N.D., HONG S.-I., KOHN D.H., *Micro- and nanostructural analyses of damage in bone*, Micron, 2005, 36, 617–629.

[83] MCCREADIE B.R., MORRIS M.D., CHEN T., SUDHAKER RAO D., FINNEY W.F., WIDJAJA E., GOLDSTEIN S.A., *Bone tissue compositional differences in women with and without osteoporotic fracture*, Bone, 2006, 39, 1190–119.

[84] BI X., PATIL CH.A., LYNCH C.C., PHARR G.M., MAHADEVAN-JANSEN A., NYMAN J.S., *Raman and mechanical properties correlate at whole bone- and tissue-levels in a genetic mouse model*, J. Biomech., 2011, 44, 297–303.

[85] JANKO M., DAVYDOVSKAYA P., BAUER M., ZINK A., STARK R.W., *Anisotropic Raman scattering in collagen bundles*, Opt. Lett., 2010, 35, 16, 2765–2767.

[86] MASIC A., BERTINETTI L., SCHUETZ R., GALVIS L., TIMOFEEVA N., DUNLOP J.W.C., SETO J., HARTMANN M.A.,

FRATZL P., *Observations of multi-scale stress-induced changes of collagen orientation in tendon by polarized Raman spectroscopy*, Biomacromolecules, 2011, (DOI: 10.1021/bm201008b).

[87] CHURCH J.S., CORINO G.L., WOODHEAD A.L., *The effect of stretching on wool fibres as monitored by FT-Raman spectroscopy*, J. Mol. Struct., 1998, 440, 1–3, 15–23.

[88] SIRICHAISIT J., YOUNG R.J., VOLLRATH F., *Molecular deformation in spider dragline silk subjected to stress*, Polym., 2000, 41, 3, 1223–1227.

[89] KOENING J.L., *Infrared and Raman Spectroscopy of Polymers*, Rapra Review Reports, Smithers Rapra Technology Limited, Shawbury, Shrewsbury, Shropshire, UK, 2001, 12, 2, Report 134.

[90] GREGORIOU V.G., BRAIMAN M.S., *Vibrational Spectroscopy of Biological and Polymeric Materials*, Boca Raton Fla London, CRC Press/Taylor& Francis Group, London, UK, 2006.

[91] WINCHESTER M.W., *Application of Raman scattering to the measurement of ligament tension*, Proceedings of the IEEE Eng. Med. Biol. Soc., 2008, 3432–3437.

[92] PRESCOTT B., STEINMETZ W., THOMAS Jr. G.J., *Characterization of DNA structures by laser Raman spectroscopy*, Biopolymers, 1984, 23, 235–256.

[93] TAILLANDIER E., LIQUIER J., GHOMI M., *Conformational transitions of nucleic acids studied by IR and Raman spectroscopies*, J. Mol. Struct., 1989, 214, 185–211.

[94] DUGUID J.G., BLOOMFIELD V.A., BENEVIDES J.M, THOMAS Jr. G.J., *Raman Spectroscopy of DNA-Metal Complexes. I. The Thermal Denaturation of DNA in the Presence of Sr2+ Ba2+ Mg2+ Ca2+ Mn2+ Co2+ Ni2+ and Cd2+*, Biophys. J, 1995, 69, 2623–2641.

[95] ERFURTH S.C., PETICOLAS W.L., *Melting and premelting phenomenon in DNA by laser Raman scattering*, Biopolymers, 1975, 14, 247–264.

[96] MOVILEANU L., BENEVIDES J.M., THOMAS Jr. G.J., *Temperature dependence of the Raman spectrum of DNA. II. Raman signatures of premelting and melting transitions of poly(dA). poly(dT) and comparison with poly(dA-dT).poly(dA-dT)*, Biopolymers, 2002, 63, 181–194.

[97] EICHHORN G.L., CLARK P., *Interactions of metal ions with polynucleotides and related compounds. V. The unwinding and rewinding of DNA strands under the influence of copper(Il) ions*, Proc. Natl. Acad. Sci., USA, 1965, 53, 586–593.

[98] EICHHORN G.L., SHIN Y.A., *Interaction of metal ions with polynucleotides and related compounds. XII. The relative effect of various metal ions on DNA helicity*, J Am. Chem. Soc., 1968, 90, 7323–7328.

[99] ANDERSON J.A., KUNTZ G.P., EVANS H.H., SWIFT T.J., *Preferential interaction of manganous ions with the guanine moiety in nucleosides dinucleoside monophosphates and deoxyribonucleic acid*, Biochemistry, 1971, 10, 4368–4374.

[100] DIX D.E., STRAUS D.B., *DMA helix stability. I. Differential stabilization by counter cations*, Arch. Biochem. Biophys., 1972, 152, 299–310.

[101] LANGLAIS M., TAJMIR-RIAHI H.A., SAVOIE R., *Raman spectroscopic study of the effects of Ca2+ Mg2+ Zn2+ and Cd2+ ions on calf thymus DNA: binding sites and conformational changes*, Biopolymers, 1990, 30, 743–752.

[102] KNOLL D.A., FRIED M.G., BLOOMFIELD V.A., *Heat-induced DNA aggregation in the presence of divalent metal salts*, [in:] M.H. Sarna and R.H. Sarna (eds.), *Structure and Expression: DNA and Its Drug Complexes Adenine*, Press Albany New York, 1988, 123–145.

[103] IYANDURAI N., SAROJINI R., *Magnesium (II) Ion Induced Changes on the Structure of DNA: An FT – Raman Study*, J. Appl. Sci. Res., 2009, 5, 283–285.

[104] DUGUID J.G., BLOOMFIELD V.A., *Aggregation of melted DNA by divalent metal ion-mediated cross-linking*, Biophysic. J., 1995, 69, 2642–2648.

[105] O'CONNOR T., MANSY S., BINA M., MCMILLIN D.R., BRUCK M.A., TOBIAS R.S., *The pH-dependent structure of calf thymus DNA studied by Raman spectroscopy*, Biophys. Chem., 1982, 15, 53–64.